Band Gap Closing in a Synthetic Hall Tube of Neutral Fermions

Jeong Ho Han, Jin Hyoun Kang, and Y. Shin*
Department of Physics and Astronomy, and Institute of Applied Physics, Seoul National University, Seoul 08826, Korea and Center for Correlated Electron Systems, Institute for Basic Science, Seoul 08826, Korea

(Received 2 September 2018; published 15 February 2019)

We report the experimental realization of a synthetic three-leg Hall tube with ultracold fermionic atoms in a one-dimensional optical lattice. The legs of the synthetic tube are composed of three hyperfine spin states of the atoms, and the cyclic interleg links are generated by two-photon Raman transitions between the spin states, resulting in a uniform gauge flux ϕ penetrating each side plaquette of the tube. Using quench dynamics, we investigate the band structure of the Hall tube system for a commensurate flux $\phi = 2\pi/3$. Momentum-resolved analysis of the quench dynamics reveals a critical point of band gap closing as one of the interleg coupling strengths is varied, which is consistent with a topological phase transition predicted for the Hall tube system.

DOI: 10.1103/PhysRevLett.122.065303

Ultracold atoms in optical lattices have become a unique platform for studying condensed matter physics in a clean and controllable environment [1,2]. Over the past decade, many experimental techniques have been demonstrated to generate artificial gauge potentials for neutral atoms, providing an interesting opportunity for exploring topologically nontrivial states of matter [3]. The Hofstadter-Harper (HH) Hamiltonian, which is the essential model for quantum Hall physics, was realized in two-dimensional (2D) optical lattice systems using laser-assisted tunneling [4–7]. Recently, ladder systems with the HH Hamiltonian, dubbed Hall ribbons, were demonstrated in the synthetic dimension framework [8,9]; in this framework, the internal degrees of freedom of atoms such as hyperfine spins [10,11] and clock states [12] are exploited as a virtual lattice dimension and the hopping along the dimension is provided by laser-induced couplings between the internal states. The framework was further extended with the external degrees of freedom of atoms such as momentum states [13–15] and lattice orbitals [16].

The key advantage of using synthetic lattice dimensions is versatile boundary manipulation. Sharp edges can be defined and individually detected with state-sensitive imaging, thus allowing for experimental investigation of various phenomena such as chiral edge currents [10,11], topological solitons at interfaces [13], and magnetic reflection [14,15]. Furthermore, nontrivial lattice geometries can be created in synthetic dimensions, which are hardly achievable with conventional optical lattices but may give rise to novel topological states [17,18]. A remarkable example is a ladder geometry with a periodic boundary condition (PBC), which can be realized by cyclically connecting the synthetic lattice sites. It is under a PBC that a Hall lattice system exhibits a true fractal structure of the single-particle energy spectrum, called Hofstadter's butterfly [19]. Additionally, Laughlin's pump, which is an ideal manifestation of quantized Hall conductivity, has been proposed for a torus geometry [20–22].

In this Letter, we report the experimental realization of a synthetic Hall lattice system of a tube geometry with ultracold fermionic atoms. In our scheme, the neutral fermions are confined in a one-dimensional (1D) optical lattice and three hyperfine spin states are employed as a synthetic dimension to form a three-leg tube structure. The cyclic links between the legs are created by spin-momentum couplings via two-photon Raman transitions between the spin states, and a uniform gauge flux $\phi = 2\pi/3$ per side plaquette is generated, thus realizing an HH Hamiltonian with a PBC [19]. Using quench dynamics, we investigate the band structure of the synthetic Hall tube system. When the system evolves from a symmetric tube to an open ladder as one of the interleg coupling strengths is decreased, we observe a critical point of band gap closing, which is consistent with a topological phase transition predicted for the Hall tube system. This work opens a new avenue for studies of topological phases with ultracold atoms in unconventional lattice geometries.

Our experiment starts with preparing a degenerate Fermi gas of ^{173}Yb atoms in the $|F = 5/2, m_F = -5/2\rangle$ hyperfine spin state of the $^1S_0$ ground energy level [23]. The typical atom number is $N \approx 1.0 \times 10^4$ and the temperature is $T/T_F \approx 0.3$, where T_F is the Fermi temperature of the trapped sample. The atoms are adiabatically loaded in a three-dimensional optical lattice potential with periodicity $d_{x,z} = \lambda_L/2$ and $d_y = \lambda_L/\sqrt{3}$, where $\lambda_L = 532$ nm is the laser wavelength. The final lattice depths are $(V_x, V_y, V_z) = (5, 20, 20)E_{L,\alpha}$, where $E_{L,\alpha} = h^2/(8md_\alpha^2)$ for $\alpha \in \{x, y, z\}$, h is the Planck constant, and m is the atomic mass. Because tunneling along the y and z directions is highly suppressed by

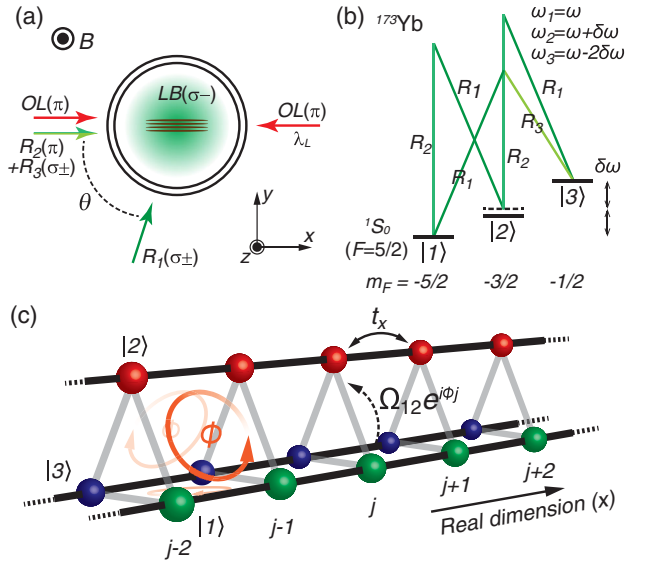

FIG. 1. Realization of a synthetic Hall tube with neutral atoms. (a) Schematic of the experimental setup. Fermionic ^{173}Yb atoms are confined in an optical lattice and illuminated by three Raman laser beams $R_{1,2,3}$. A magnetic field B and an additional laser light (LB) are applied along $\hat{z}$ to control the energy levels of the spin states. (b) The three lowest spin states of ^{173}Yb are coupled to each other via two-photon Raman transitions by $R_{1,2,3}$. (c) Synthetic three-leg Hall tube with a uniform gauge flux ϕ on each side plaquette. The three legs are formed by the three spin states of the atoms in the 1D optical lattice (black lines) and the interleg tunneling with complex amplitude (gray lines) is provided by the cyclic Raman couplings between the spin states.

large lattice depths, our lattice system is effectively one dimensional. The tunneling amplitude is $t_x = 2\pi \times 264$ Hz, and the characteristic filling factor is estimated to be ≈ 0.75 with trapping frequencies of $(\omega_x, \omega_y, \omega_z) = 2\pi \times (58, 42, 132)$ Hz [2,24]. An external magnetic field of 153 G is applied along $\hat{z}$ to lift the spin degeneracy of the $^1S_0$ energy level.

The three lowest spin states, which we denote $|1\rangle \equiv |m_F = -5/2\rangle$, $|2\rangle \equiv |m_F = -3/2\rangle$, and $|3\rangle \equiv |m_F = -1/2\rangle$, are employed for the three legs of the synthetic tube system. To generate interleg couplings, three linearly polarized Raman laser beams $R_{1,2,3}$ are irradiated on the sample [Fig. 1(a)], where the wave vectors of the laser beams are given by $\vec{k}_{r1} = k_R(\cos\theta\hat{x} + \sin\theta\hat{y})$ and $\vec{k}_{r2} = \vec{k}_{r3} = k_R\hat{x}$, respectively, and the polarization directions are horizontal for $R_{1,3}$ and vertical for R_2 to the xy plane. The laser frequencies of $R_{1,2,3}$ are set to $\omega_1 = \omega$, $\omega_2 = \omega + \delta\omega$, and $\omega_3 = \omega - 2\delta\omega$, respectively, where ω is the laser frequency blue-detuned by 1.97 GHz from the $|^1S_0, F = 5/2\rangle \rightarrow |^3P_1, F' = 7/2\rangle$ transition line. When $\delta\omega$ is tuned to half of the energy difference between $|1\rangle$ and $|3\rangle$, the three spin states $\{|1\rangle, |2\rangle, |3\rangle\}$ can be resonantly coupled to each other in a cyclic manner by two-photon Raman transitions, as described in Fig. 1(b). Thus, a three-leg synthetic tube is constructed with the fermions in the 1D optical lattice [Fig. 1(c)].

In the synthetic tube system, the Raman coupling between the spin states $|s\rangle$ and $|s'\rangle$ is described by interleg tunneling with complex amplitude $\Omega_{ss'}e^{i\phi j}$, where $\Omega_{ss'}$ is the Rabi frequency of the corresponding Raman transition and j is the site index for the real lattice. The spatial phase modulations of the tunneling amplitude originate from the momentum transfer $\hbar\Delta\vec{k}$ of the two-photon transition, yielding $\phi = (\Delta\vec{k}\cdot\hat{x})d_x$ [7]. In our setup, $\Delta\vec{k} = \vec{k}_{r2,r3} - \vec{k}_{r1} = k_R[(1-\cos\theta)\hat{x} - \sin\theta\hat{y}]$ for all the cyclic interleg couplings and $\phi = 2\pi k_R d_x(1-\cos\theta)$ regardless of spin state. When a fermion hops around any side plaquette of the tube, it acquires a uniform net phase of ϕ, thus realizing the HH Hamiltonian in the tube geometry. In this work, we set $\theta \approx 72°$ to have $\phi = 2\pi/3$, satisfying the PBC for the synthetic dimension. Because the σ-σ transition ($\Delta m_F = 2$) for the $|1\rangle - |3\rangle$ coupling is relatively weak, the intensity ratio of $R_{1,2,3}$ is adjusted to create a symmetric coupling structure. We measure $\Omega_{12} = \Omega_{31} \approx 12.3t_x$. Here, Ω_{23}/Ω_{12} is fixed because the π-σ ($\Delta m_F = 1$) transitions for the $|1\rangle$–$|2\rangle$ and $|2\rangle$–$|3\rangle$ couplings are created by the same pair of Raman beams, and the ratio is nearly unity within 2%.

In realizing the three-leg Hall tube, careful control of the energy levels ν_s of the spin states is necessary to suppress the optical transitions to the other spin states, $|4\rangle \equiv |m_F = 1/2\rangle$ and $|5\rangle \equiv |m_F = 3/2\rangle$. In addition to the magnetic Zeeman shift, ν_s is adjusted with a differential ac Stark shift by radiating an additional laser light along $\hat{z}$ [25], which is σ^- polarized and detuned by -70 MHz with respect to the $|^1S_0, F = 5/2\rangle \rightarrow |^3P_1, F' = 7/2\rangle$ transition line. Under the final experimental condition, the energy level differences between the spin states are spectroscopically measured [26] and $(\xi_1, \xi_2, \xi_3, \xi_4, \xi_5) \approx (0, -0.2, 0, -2, 1.7)\Omega_{12}$, where $\xi_s = (\nu_s - \nu_1) - (s-1)\delta\omega$ and $\delta\omega = 2\pi \times 30.4$ kHz. ξ_s is the detuning of $|s\rangle$ from the energy staircase formed by two-photon Raman processes with a step unit of $\delta\omega$. The atom loss rate into $|4\rangle$ and $|5\rangle$ is measured to be $\approx 0.01\Omega_{12}$.

The Bloch Hamiltonian of the Hall tube system is given by

$$\hat{H}_q/\hbar = \begin{pmatrix} -2t_x\cos(q-\phi) & \Omega_{12}/2 & \Omega_{31}/2 \\ \Omega_{12}/2 & \xi_2 - 2t_x\cos(q) & \Omega_{23}/2 \\ \Omega_{31}/2 & \Omega_{23}/2 & -2t_x\cos(q+\phi) \end{pmatrix}, \quad (1)$$

where q is the quasimomentum of the lattice tube system normalized by d_x^{-1} [26]. For a symmetric case with $\Omega_{12} = \Omega_{23} = \Omega_{31}$ and $\xi_2 = 0$, the Hamiltonian $\hat{H}_q$ for $\phi = 2\pi/3$ embeds a topologically nontrivial state, which is protected by a generalized inversion symmetry [18,28]. In our experiment, this symmetry is preserved with spatially uniform $\Omega_{ss'}$ and the topological state survives $\xi_2 \neq 0$, featuring a nonzero Zak phase $Z = 1$ of its lowest band [29]. In $\hat{H}_q$, time-reversal symmetry, particle-hole symmetry, and chiral symmetry are broken, which corresponds to the symmetry class A (unitary) of the Altland-Zirnbauer classification [30,31]. When the lowest band is completely filled, the system represents a topological insulating state analogous to the integer quantum Hall state [32].

To demonstrate the presence of a gauge flux on plaquettes, we investigate the quench dynamics of the synthetic Hall system. Atoms are initially prepared in $|1\rangle$, and then the interleg couplings are suddenly activated by turning on the Raman laser beams. After a variable hold time, the spin composition is measured by imaging with optical Stern-Gerlach spin separation [33], and separately, the lattice momentum distribution $n(k)$ is measured using an adiabatic band-mapping technique [24,26]. Note that in the band-mapping process, the quasimomentum state with q is transformed into a superposition of free-space momentum states of the three spin states in the first Brillouin zone (BZ), where the momentum k_s of spin state $|s\rangle$ is related to q as $k_s d_x = [q + (s-2)\phi]$ modulo 2π and $-k_L < k_s \leq k_L$ with $k_L = \pi/d_x$. The momentum distribution $n_s(k)$ of the atoms in $|s\rangle$ is also measured by spin-selective imaging [Fig. 2(b)] [23].

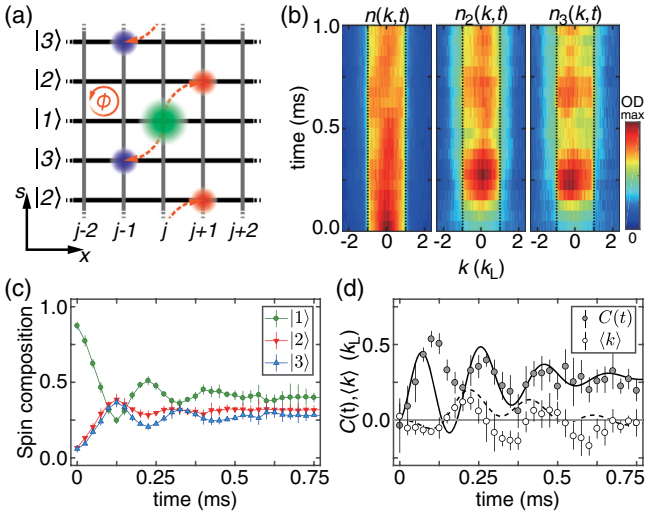

FIG. 2. Quench dynamics of the three-leg Hall tube for $\phi = 2\pi/3$. (a) Illustration of the atomic motion in the Hall tube. Atoms are initially prepared in the spin-$|1\rangle$ leg and the interleg couplings are suddenly activated. (b) Time evolution of the lattice momentum distribution $n(k,t)$ of the sample, $n_2(k,t)$ of the atoms in $|2\rangle$, and $n_3(k,t)$ of the atoms in $|3\rangle$. Time evolution of (c) the fractional spin populations, (d) the average lattice momentum $\langle k\rangle$ of the sample, and the difference $\mathcal{C}(t) = \langle k_2\rangle - \langle k_3\rangle$ between the momenta of the two legs $|2\rangle$ and $|3\rangle$. Each data point comprises five measurements of the same experiment, and the error bar is their standard deviation. The solid and dashed lines in (d) show the numerical simulation results for $\mathcal{C}$ and $\langle k\rangle$, respectively [26].

The measurement results of the time evolution of the quenched synthetic Hall tube system are displayed in Figs. 2(c) and 2(d). At the early time $t < 100\ \mu$s, when the atoms start transferring to $|2\rangle$ and $|3\rangle$, the average lattice momentum of the sample, $\langle k\rangle = \int_{-k_L}^{k_L} kn(k)dk / \int_{-k_L}^{k_L} n(k)dk$, shows no significant variations; however, the difference between the momenta of the atoms transferred into $|2\rangle$ and $|3\rangle$, $\mathcal{C}(t) = \langle k_2\rangle - \langle k_3\rangle$, where $\langle k_s\rangle = \int_{-k_L}^{k_L} kn_s(k)dk / \int_{-k_L}^{k_L} n_s(k)dk$, increases noticeably. This means that the atoms in the legs $|2\rangle$ and $|3\rangle$ move in positive and negative directions of the real lattice, respectively, which is understandable based on the classical motion of a charged particle moving in the tube in the presence of a magnetic field [Fig. 2(a)]. At later times, the spin composition and $\mathcal{C}(t)$ show damped oscillations, which are reasonably accounted for by a numerical simulation for $\hat{H}_q$ including phenomenological damping [26]. The asymmetry between $|2\rangle$ and $|3\rangle$ and the small oscillations of $\langle k\rangle$ result from nonzero ξ_2.

The quench evolution of the Hall system is further examined for open ladder geometries [Figs. 3(a) and 3(b)].

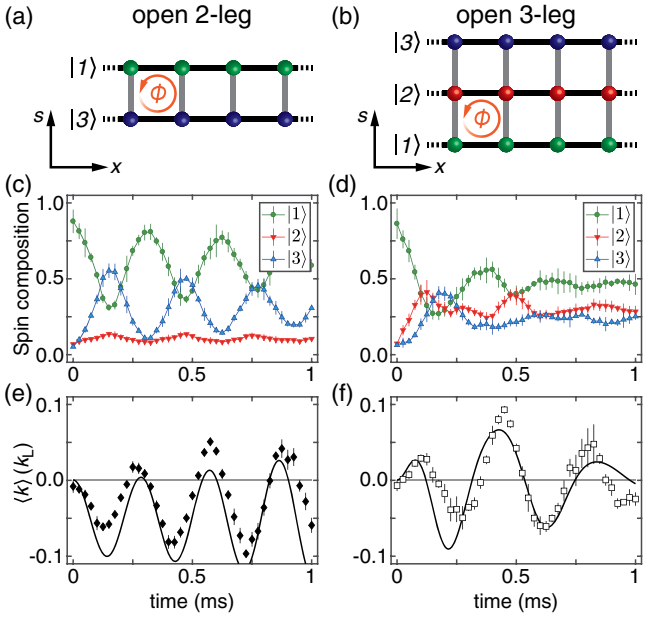

FIG. 3. Quench dynamics of (a) two-leg and (b) three-leg ladders with open boundaries for $\phi = 2\pi/3$. Time evolution of (c),(d) the fractional spin populations and (e),(f) the average lattice momentum $\langle k\rangle$. The solid lines display the numerical simulation results for $\langle k\rangle$ [26]. Each data point comprises five measurements of the same experiment, and the error bar is their standard deviation.

The structure modification is achieved by deactivating two or one of the interleg links; by shifting ω_2 (ω_3) by $2\pi \times 400$ (-400) kHz, a two-(three-)leg ladder is formed. For large detuning, the associated interleg couplings are effectively turned off but the ac Stark shifts due to the Raman beams are nearly unaffected [34,35]. The time evolutions of the spin composition and $\langle k \rangle$ are displayed in Figs. 3(c)–3(f). In contrast to the Hall tube case, $\langle k \rangle$ shows relatively large oscillations because the atoms are initially prepared at an edge of the ladder. Interestingly, $\langle k \rangle$ changes its sign during the oscillations. The behavior is also observed in the numerical simulations [Figs. 3(e) and 3(f)], and we attribute it mainly to the large gauge flux $\phi > \pi/2$ causing atoms to reflect at the BZ boundary. We note that the sign change of $\langle k \rangle$ was not observed in previous experiments for a smaller gauge flux [10]. The semiclassical trajectories of the open ladder systems reveal characteristic cyclotron motions [26], corroborating the presence of a gauge flux on the side plaquettes of the synthetic tube.

In Fig. 4(a), we present the phase diagram of the Hall tube system for $\phi = 2\pi/3$ in the plane of Ω_{12} and Ω_{31}. The topological phase with $Z = 1$ exists in a region of $\Omega_- < \Omega_{31} < \Omega_+$, where $\Omega_\pm = \pm 3t_x - \xi_2 + \sqrt{(3t_x \mp \xi_2)^2 + \Omega_{12}^2}$. Our current system with $\Omega_{31} = \Omega_{12} \approx 12.3t_x$ is located in the topological regime and its transition to a topologically trivial phase with $Z = 0$ can be driven by, e.g., decreasing Ω_{31} below the critical value of $\Omega_- = 11.6t_x$ [18]. In Fig. 4(b), the band dispersions of the Hall tube system are displayed for various Ω_{31}, showing that the topological phase transition at $\Omega_{31} = \Omega_-$ occurs with closing the energy gap between the first and second bands at quasimomentum $q_c = \pm\pi$ [36].

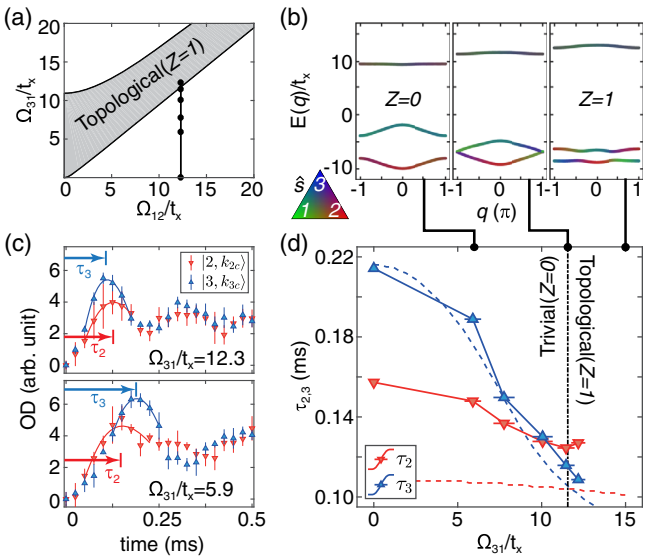

FIG. 4. Observation of band gap closing in the Hall tube. (a) Phase diagram in the plane of Ω_{12} and Ω_{31}. The shaded area indicates a topologically nontrivial phase with a nonzero Zak phase $Z = 1$ of the lowest band. The solid dots indicate the positions explored in the experiment. (b) Band structures calculated for various Ω_{31} with $\Omega_{12} = \Omega_{23} \approx 12.3t_x$. A topological phase transition occurs together with band gap closing at $q_c = \pm\pi$. (c) Quench evolution of $n_2(k_{2c})$ and $n_3(k_{3c})$, where k_{2c} and k_{3c} are the lattice momenta of $|2\rangle$ and $|3\rangle$, respectively, corresponding to q_c. Each data point is obtained by averaging five measurements and the error bar is their standard deviation. The time τ_2 (τ_3) for the first maximum of $n_2(k_{2c})$ [$n_3(k_{3c})$] is determined by fitting the experimental data to an asymmetric parabola function (solid line). (d) τ_2 and τ_3 as functions of Ω_{31}. The red and blue dashed lines show the numerical results for τ_2 and τ_3, respectively. $\tau_2 = \tau_3$ indicates the critical point of band gap closing.

The critical point of band gap closing is probed via momentum-resolved analysis of the quench dynamics. As the band gap closes, the dynamic evolution for $q = q_c$ is governed by a single energy scale that is determined by the energy difference between the third band and the two touching lowest bands. Therefore, the gap closing would be characteristically reflected in the quench evolution of the spin composition at q_c. The momenta of the spin states $|2\rangle$ and $|3\rangle$ corresponding to $q_c = \pm\pi$ are $k_{2c} = -k_L$ and $k_{3c} = -k_L/3$, respectively, and we measure the quench evolution of $n_2(k_{2c})$ and $n_3(k_{3c})$ for various $\Omega_{31} \leq \Omega_{12}$ [Fig. 4(c)]. When Ω_{31} is decreased by decreasing the intensity of R_3, the resulting reduction of the ac Stark shift is compensated for by applying another off-resonant laser light with the same polarization as R_3. To obtain the characteristic timescales of the spin composition oscillations, we determine the times τ_2 and τ_3 at which $n_2(k_{2c})$ and $n_3(k_{3c})$ reach their first maxima, respectively, by fitting the experimental data to an asymmetric parabolic function [37].

Figure 4(d) shows the measurement results of $\tau_{2,3}$ as functions of Ω_{31}. At $\Omega_{31} = \Omega_{12}$, τ_3 is smaller than τ_2 and as Ω_{31} decreases, it increases faster than τ_2. The crossing of τ_2 and τ_3 occurs at $\Omega_{31} \approx 10.4t_x$ in the vicinity of the expected critical point Ω_-. The numerical simulation reproduces the observed crossing behavior and yields $\tau_2 = \tau_3$ at $\Omega_{31} = \Omega_-$, which validates our experimental approach using the time scales of quench dynamics to probe band gap closing. It might be speculated that the deviation of the measured critical value from the predicted Ω_- is possibly associated with the renormalization by interaction effects [38]. For our experimental parameters, the on-site interaction energy is estimated to be $U/\hbar \approx 1.7t_x$. However, the deviation is prominent only in τ_2, which suggests that it might be due to technical imperfections in our spin-selective imaging.

In conclusion, we realize a synthetic three-leg Hall tube with $\phi = 2\pi/3$ and demonstrate the band gap closing at a critical point of the topological phase transition of the system. In our experimental setup, the gauge flux ϕ can be controlled by the intersection angle θ between the Raman beams, and we expect an immediate expansion of this work to study fractal band structures with varying magnetic fluxes from commensurate to incommensurate values. Further studies may include interatomic interactions [39],

which are expected to show fractional charge behavior [21], using the recently implemented orbital Feschbach resonance [40,41].

We thank Moosong Lee for early contributions to this work and Seji Kang for experimental assistance. This work is supported by the Institute for Basic Science (IBS-R009-D1) and the National Research Foundation of Korea (Grants No. NRF-2018R1A2B3003373 and No. 2014-H1A8A1021987).

*yishin@snu.ac.kr

[1] D. Jaksch and P. Zoller, Ann. Phys. (Amsterdam) **315**, 52 (2005).
[2] I. Bloch, J. Dalibard, and W. Zwerger, Rev. Mod. Phys. **80**, 885 (2008).
[3] J. Dalibard, F. Gerbier, G. Juzeliūnas, and P. Öhberg, Rev. Mod. Phys. **83**, 1523 (2011).
[4] M. Aidelsburger, M. Atala, M. Lohse, J. T. Barreiro, B. Paredes, and I. Bloch, Phys. Rev. Lett. **111**, 185301 (2013).
[5] H. Miyake, G. A. Siviloglou, C. J. Kennedy, W. C. Burton, and W. Ketterle, Phys. Rev. Lett. **111**, 185302 (2013).
[6] Y.-J. Lin, K. Jiménez-García, and I. B. Spielman, Nature (London) **471**, 83 (2011).
[7] N. Goldman, G. Juzeliūnas, P. Öhberg, and I. B. Spielman, Rep. Prog. Phys. **77**, 126401 (2014).
[8] O. Boada, A. Celi, J. I. Latorre, and M. Lewenstein, Phys. Rev. Lett. **108**, 133001 (2012).
[9] A. Celi, P. Massignan, J. Ruseckas, N. Goldman, I. B. Spielman, G. Juzeliūnas, and M. Lewenstein, Phys. Rev. Lett. **112**, 043001 (2014).
[10] M. Mancini, G. Pagano, G. Cappellini, L. Livi, M. Rider, J. Catani, C. Sias, P. Zoller, M. Inguscio, M. Dalmonte, and L. Fallani, Science **349**, 1510 (2015).
[11] B. K. Stuhl, H.-I. Lu, L. M. Aycock, D. Genkina, and I. B. Spielman, Science **349**, 1514 (2015).
[12] L. F. Livi, G. Cappellini, M. Diem, L. Franchi, C. Clivati, M. Frittelli, F. Levi, D. Calonico, J. Catani, M. Inguscio, and L. Fallani, Phys. Rev. Lett. **117**, 220401 (2016).
[13] E. J. Meier, F. A. An, and B. Gadway, Nat. Commun. **7**, 13986 (2016).
[14] F. A. An, E. J. Meier, and B. Gadway, Sci. Adv. **3**, e1602685 (2017).
[15] F. A. An, E. J. Meier, and B. Gadway, Nat. Commun. **8**, 325 (2017).
[16] J. H. Kang, J. H. Han, and Y. Shin, Phys. Rev. Lett. **121**, 150403 (2018).
[17] O. Boada, A. Celi, J. Rodríguez-Laguna, J. I. Latorre, and M. Lewenstein, New J. Phys. **17**, 045007 (2015).
[18] S. Barbarino, M. Dalmonte, R. Fazio, and G. E. Santoro, Phys. Rev. A **97**, 013634 (2018).
[19] D. R. Hofstadter, Phys. Rev. B **14**, 2239 (1976).
[20] R. B. Laughlin, Phys. Rev. B **23**, 5632 (1981).
[21] T.-S. Zeng, C. Wang, and H. Zhai, Phys. Rev. Lett. **115**, 095302 (2015).
[22] L. Taddia, E. Cornfeld, D. Rossini, L. Mazza, E. Sela, and R. Fazio, Phys. Rev. Lett. **118**, 230402 (2017).
[23] M. Lee, J. H. Han, J. H. Kang, M.-S. Kim, and Y. Shin, Phys. Rev. A **95**, 043627 (2017).
[24] M. Köhl, H. Moritz, T. Stöferle, K. Günter, and T. Esslinger, Phys. Rev. Lett. **94**, 080403 (2005).
[25] B. Song, L. Zhang, C. He, T. F. J. Poon, E. Hajiyev, S. Zhang, X.-J. Liu, and G.-B. Jo, Sci. Adv. **4**, eaao4748 (2018).
[26] See Supplemental Material at http://link.aps.org/supplemental/10.1103/PhysRevLett.122.065303 for the details of experimental sequence, measurement of energy level difference, the tight-binding model description, the semiclassical trajectory data, and numerical simulations, which includes Ref. [27].
[27] J. Heinze, S. Götze, J. S. Krauser, B. Hundt, N. Fläschner, D.-S. Lühmann, C. Becker, and K. Sengstock, Phys. Rev. Lett. **107**, 135303 (2011).
[28] H. L. Nourse, I. P. McCulloch, C. Janani, and B. J. Powell, Phys. Rev. B **94**, 214418 (2016).
[29] J. Zak, Phys. Rev. Lett. **62**, 2747 (1989).
[30] A. Altland and M. R. Zirnbauer, Phys. Rev. B **55**, 1142 (1997).
[31] C.-K. Chiu, J. C. Y. Teo, A. P. Schnyder, and S. Ryu, Rev. Mod. Phys. **88**, 035005 (2016).
[32] A. P. Schnyder, S. Ryu, A. Furusaki, and A. W. W. Ludwig, Phys. Rev. B **78**, 195125 (2008).
[33] S. Taie, Y. Takasu, S. Sugawa, R. Yamazaki, T. Tsujimoto, R. Murakami, and Y. Takahashi, Phys. Rev. Lett. **105**, 190401 (2010).
[34] P. Wang, Z.-Q. Yu, Z. Fu, J. Miao, L. Huang, S. Chai, H. Zhai, and J. Zhang, Phys. Rev. Lett. **109**, 095301 (2012).
[35] L. W. Cheuk, A. T. Sommer, Z. Hadzibabic, T. Yefsah, W. S. Bakr, and M. W. Zwierlein, Phys. Rev. Lett. **109**, 095302 (2012).
[36] For $\Omega_{12} = \Omega_{23}$, $\hat{H}_q$ is mirror symmetric along spin dimension with respect to $|2\rangle$, and therefore, the quasimomentum for gap closing should be $q = 0$ or $\pm\pi$. Here, the topological transition at $\Omega_{31} = \Omega_+$ shows the gap closing at $q = 0$.
[37] The fitting function is given by $f(t) = \alpha_1(t - \tau_s)^2 + \beta$ for $t \leq t_s$ and $\alpha_2(t - \tau_s)^2 + \beta$ for $t > t_s$ with four fitting parameters, $\alpha_{1,2}$, β, and τ_s.
[38] S. Barbarino, L. Taddia, D. Rossini, L. Mazza, and R. Fazio, New J. Phys. **18**, 035010 (2016).
[39] S. Barbarino, L. Taddia, D. Rossini, L. Mazza, and R. Fazio, Nat. Commun. **6**, 8134 (2015).
[40] G. Pagano, M. Mancini, G. Cappellini, L. Livi, C. Sias, J. Catani, M. Inguscio, and L. Fallani, Phys. Rev. Lett. **115**, 265301 (2015).
[41] M. Höfer, L. Riegger, F. Scazza, C. Hofrichter, D. R. Fernandes, M. M. Parish, J. Levinsen, I. Bloch, and S. Fölling, Phys. Rev. Lett. **115**, 265302 (2015).